REVEALING THE DEVELOPMENT OF LOCAL HOLLOWINGS IN RINNENKARREN USING FIELD DATA (TOTES GEBIRGE, AUSTRIA) AND SIMULATION OF DIFFERENT NUMBERS OF CHANNEL JUNCTIONS

RAZKRIVANJE RAZVOJA LOKALNIH VDOLBIN V ŽLEBIČIH NA PODLAGI TERENSKIH PODATKOV (VISOKE TURE (TOTES GEBIRGE), AVSTRIJA) IN SIMULACIJE RAZLIČNEGA ŠTEVILA KANALSKIH STIČIŠČ

Mitre ZOLTÁN[1] & Veress MÁRTON[2]

Abstract UDC 551.311.2:551.435.81:004.94
Mitre Zoltán & Veress Márton: Revealing the development of local hollowings in rinnenkarren using field data (Totes Gebirge, Austria) and simulation of different numbers of channel junction
The development of emerging hollowing parts of the main channels of rinnenkarren systems at tributary channel junctions is interpreted in this study using Computational Fluid Dynamics (CFD) simulation. In the field, data from cross-sections of 505 local hollowings with one or more tributary channel junctions were investigated. The shift in the width–depth ratio of the local hollowings was studied as the number of junctions and the size of the hollowing changed. Flow was simulated through CFD in digital model channels, and the nature of the resulting vorticity was interpreted. Field data show that local hollowings emerging in the main channels of the channel systems at the junctions. In the main channels, when only a few tributary channels join in the vicinity of each other, local hollowings deepen during their growth and, most often, gradually become pits (depth is larger than width), as the morphometric analysis suggests. As the number of tributary channels increases, the local hollowing may develop into a kamenitza (width is larger than depth). The model experiment suggests the explanation that more tributary channel junctions result in more extensive vorticity, which contributes to the lateral extension (widening) of this channel section. The distance of the tributary junctions from each other

Izvleček UDK 551.311.2:551.435.81:004.94
Mitre Zoltán & Veress Márton: Razkrivanje razvoja lokalnih vdolbin v žlebičih na podlagi terenskih podatkov (Visoke Ture (Totes Gebirge), Avstrija) in simulacije različnega števila kanalskih stičišč
Razvoj nastajajočih votlih delov glavnih kanalov v sistemih žlebičev na kanalskih stičiščih pritokov je v tej študiji razložen s simulacijo računalniške dinamike tekočin (CFD). Na terenu so bili proučeni podatki iz prečnih prerezov 505 lokalnih vdolbin z enim ali več stičišč pritočnih kanalov. Raziskana je bila sprememba razmerja med širino in globino lokalnih vdolbin glede na spremembe tako števila stičišč kot velikosti vdolbine. Pretok je bil s CFD simuliran v digitalnih modelnih kanalih, nato pa je bila pojasnjena narava nastalega vrtinčenja. Terenski podatki kažejo, da se v glavnih kanalih kanalnih sistemov na stičiščih pojavljajo lokalne vdolbine. V glavnih kanalih, kjer se v bližini drug drugega združi le nekaj pritočnih kanalov, se lokalne vdolbine sčasoma poglabljajo in najpogosteje postopno postanejo jame (globina je večja od širine), kot je razvidno iz morfometrične analize. S povečevanjem števila pritočnih kanalov se lahko lokalna vdolbina razvije v škavnico (širina je večja od globine). Na podlagi modelnega poskusa se predlaga razlaga, da več stičišč pritočnih kanalov povzroči obsežnejše vrtinčenje, ki prispeva k lateralni širitvi (razširitvi) zadevnega odseka kanala. Na velikost lokalne vdolbine v smeri toka vpliva tudi medsebojna oddaljenost stičišč pritočnih kanalov. Na terenu je opazno, da večja ko je ta razdalja,

[1] Institute of Geography and Earth Sciences, Faculty of Sciences, University of Pécs. H-7624 Pécs, Ifjúság útja 6. (Hungary).
E-mail: zoltan.mitre@gmail.com
[2] Savaria Department of Geography, Eötvös Loránd University. H-9700 Szombathely, Károlyi Gáspár tér 4. (Hungary).
E-mail: veress.marton@sek.elte.hu

also influences the downstream dimension of the local hollowing. In the field, the larger this distance, the more separated the local hollowings induced by individual tributaries. The model experiment suggests that this may occur because the intense vorticity generated by individual junctions becomes increasingly sectionalized as the tributary channel density decreases.

Keywords: rinnenkarren, tributary channel, local hollowing, cross-section increase, CFD simulation, vorticity.

bolj so lokalne vdolbine, ki jih povzročajo posamezni pritoki, oddaljene druga od druge. Iz modelnega poskusa je razvidno, da se to lahko zgodi, ker se intenzivno vrtinčenje, ki nastane na posameznih stičiščih, z zmanjševanjem gostote pritočnih kanalov vedno bolj razdeli v segmente.

Ključne besede: žlebiči, pritočni kanal, lokalna vdolbina, povečanje prečnih prerezov, simulacija z računalniško dinamiko tekočin (CFD), vrtinčenje.

1. INTRODUCTION

In this study cross-section development of channel systems is interpreted at single and multiple tributary channel junctions with the help of Computational Fluid Dynamics (CFD) simulation. Rinnenkarren are closed downhill arheic channels of dissolution origin, developed by rivulets (Figure 1, Sweeting, 1973; Trudgill, 1985; White, 1988; Hutchinson, 1996; Ford & Williams 2007; Veress, 2010). The channel systems (Horton-type channels, Ford & Williams, 1989, 2007) consist of a large main channel (often up to 30-50 m long) and joining smaller-sized tributary channels (Veress et al., 2013, 2015a). Their widths and depths are a few decimeters at the most. Usually, the cross-section of the channels increases gradually downslope from the top of the slope (Veress, 2010).

However, the increase in channel cross-section of the main channel can also occur locally at the tributary channel junctions (local hollowing), along short sections (≈0.3-1 m, Veress et al., 2013). Kamenitzas with various morphologies (Veress, 2010) often appear in these places as well, which may be connected here to several tributary channels. The origin of local hollowing is attributed to flow with emerged vorticity at the junctions (Veress et al., 2013). The vorticity at the site of the junctions was confirmed by laboratory model experiments (Deák et al., 2012).

The mentioned previous studies as well as the recent ones (Veress et al., 2019) did not cover all the characteristics of the development of local hollowings at multichannel junctions. Studies of flow conditions in the field are limited. The formation of rivulets in channels, and hence their effect(s), could only be observed during snow melt (or permanent, significant rainfall) when the field is difficult or even impossible to access.

Recently, numerical simulations and CFD (Jiyuan et al., 2013) became more widespread and opened up new possibilities to study geomorphic problems (Bates et al., 2005) as well. Some numerical models were successfully applied to the examination of caves (including the increase of the channels, Perne et al., 2014; Covington & Perne, 2015). However, these were also applied to karst hydrology (Zhao et al., 2019) and speleogenesis (Dreybrodt et al., 2005; Cooper & Covington, 2020). In this study CFD simulation is also used for improving a previous model (Veress et al., 2013) of channel local hollowing development.
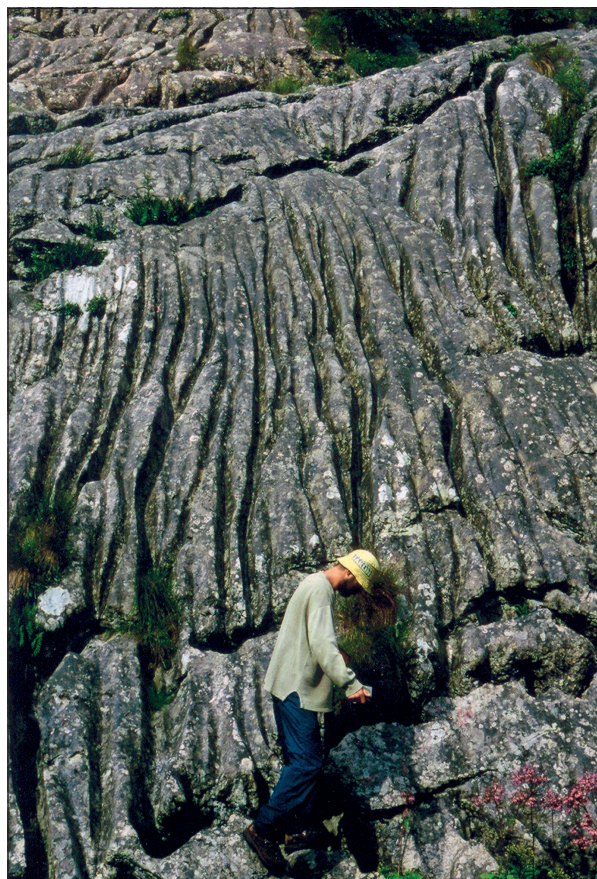

Figure 1: Rinnenkarren with only a few tributary channels, Julian Alps, Slovenia.

Figure 2: The location of studied channels in the Totes Gebirge on a sketch map about the study site. Legend: 1. lake; 2. tourist trail; 3. hostel; 4. peak; 5. studied channel area.

2. DATA AND BACKGROUND

2.1. STUDY SITE

The rinnenkarren used in this study were surveyed in Totes Gebirge, Austria (Figure 2, Veress et al., 2013, 2019) between 1993-2016. Totes Gebirge is a part of the Northern Limestone Alps, which is the remnant frontal part of the Upper Austrian Prealps nappe and belongs to the unit of Tirolean Facies. Totes Gebirge is straddled by the Ennstal Alps and Dachstein and Traunstein mountains. It is built up of limestone, in the west of Triassic (werfen, dachstein), and in the east of Jurassic age (Plan et al., 2009). The bedrock of the study site is Dachstein limestone. The mountain, from a morphologic aspect, is a glaciokarst, characterized by glacier valleys, scablands, horns, and also dolines of different types and epochs (Veress, 2016). However, its most characteristic karst forms are karren which mainly occur both on the slopes and bottoms of glacier valleys in the Dachstein limestone, which can be regarded as homogeneous. Karren appears especially where the ice carved stepped pavement surfaces. Rinnenkarren appear on gently sloping bed plane surfaces of steps (Veress, 2010; Veress et al., 2019).

2.2. MORPHOLOGY

A single tributary channel (single junction) or several tributary channels within a short stretch (within 1 m, multiple junctions, Figure 3a) can be adjoined to the main channel of a channel system (Figure 3a). Ridges of different width are present between the main and tributary channels (Figure 3b), which are the remnants of the original terrain (Veress, 2010).

Local hollowings develop in the main channel in the vicinity of the junctions. A local hollowing means clearly distinguishable cross-section growth along a stretch with a given length (D_T, Figure 3b, Veress et al., 2013). Hollowings can further turn into pits or kamenitzas. In the field, examples can be found for both features (Veress, 2010). In the case of channels, both of these features can be exactly defined as "Rinnenkarren-interrupting kamenitza- or pit-like features". However, previous studies simply refer to them as kamenitzas and pits. For ease of reference the latter names are used here.

A karren feature can be regarded as a kamenitza when its width is larger than its depth and to pit when its depth larger than its width. The morphology of kamenitzas is various; their walls can be steep or bending. Within channel systems often multiple tributaries join them (Veress, 2010). Some kamenitzas are in the lowest downchannel position, while in other cases, the kamenitzas are extreme hollowings of the main channel. Here feeding channels converge (multiple junctions).

In the case of multiple junctions, a continuous local hollowing of the main channel typically appears along its section with tributary channels. This kind of local hol-lowing section is also well separated from the smaller cross-sectional main channel sections without any tributary channel.

The width-depth ratio of a given cross-section (A^*) of channel and local hollowing indicates the relation between width (Δx, Figure 3b) and depth (Δz, Figure 3b) which can be given with

$$A^* = \frac{\Delta x}{\Delta z} \qquad (1)$$

expression (Figure 3b, Veress et al., 2013). The cross-section shape of the channels in the nearest approach is of a "U" shape (Veress, 2010), but it was approximated with an ellipse (Szunyogh, 1995) as well. Cross-section area (T^*) of the channels at a given cross-section is width multiplied with depth as

$$T^* = \Delta x \cdot \Delta z \qquad (2)$$

(Figure 3b, Veress et al., 2013).

2.3. CHANNEL PROPERTIES AND MEASUREMENT

In the course of the field surveys in the Totes Gebirge, 70 channel systems were investigated. These included a total of 781 tributary channel junctions. The width (Δx, Figure 3b) and depth (Δz, Figure 3b) of main channels were measured with a tape measure along profiles at a distance of 0.1 m. The width and depth data of channels are given to an accuracy of 0.01 m from the field.

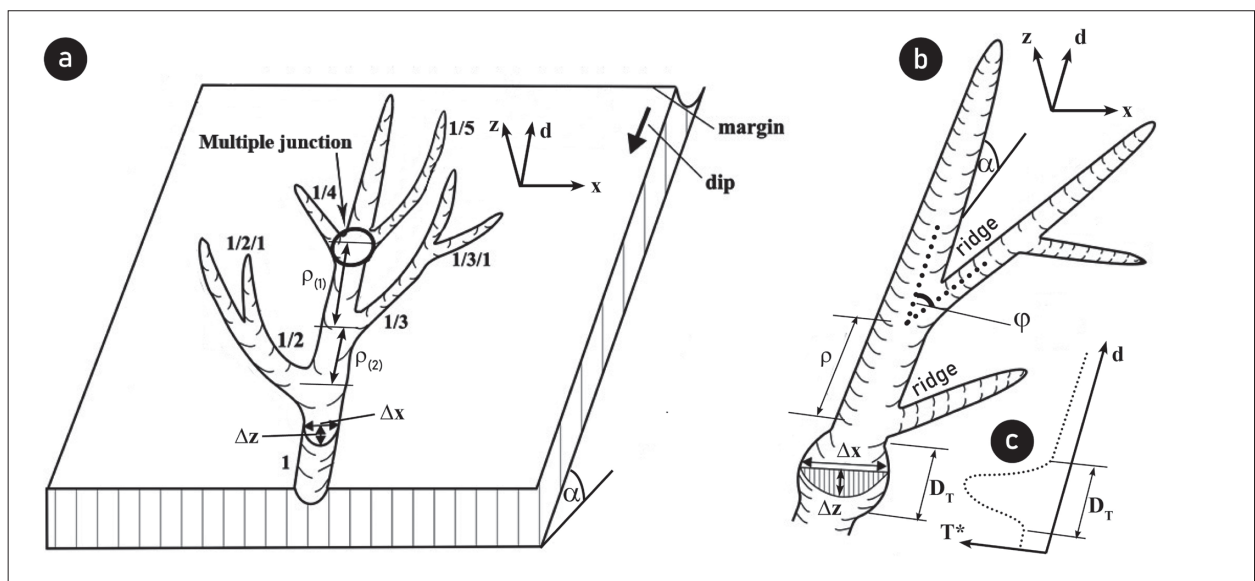The field database contains 505 local hollowings

Figure 3: Sketch of a rinnenkarren system and its morphometric parameters based on Veress et al. (2013). Signs: (Δx) channel width; (Δz) channel depth; (D_T) length of local hollowing; (ρ) distance of the tributary channel junctions; (φ) junction angle of the tributary channel; (α) slope angle; (T^*) cross-section area of the main channel across a given measurement profile; (d) distance along the main channel from its bottom part.

joined by a single or several tributary channels. Local hollowing lengths were measured directly during the field surveys with an accuracy of 0.01 m. This is the D_T section length.

The slope angle (α, Figure 3) of the sites was measured along the same profiles of width and depth data measurements using a slope meter, also a geological compass. It was also determined from the data of a right triangle (based on the leg opposite the angle and the hypotenuse) formed at a horizontal distance of 1 m.

The tributary channels join to the main channel with variable junction angles (φ, Figure 3) but not more than 90°. The angle between the center line of the channels gives the junction angle (φ, Figure 3) which was measured directly with a protractor of appropriate size.

The depth of the wet cross-section in channels without any junctions should not exceed 0.1 m as assumed from previous analyses (Szunyogh, 1995) in the study area. Furthermore, the steady-state flow velocity without any junction is around 1 ms^{-1}. Laboratory experiments (Veress et al., 2013, 2015b) measured similar steady state flow velocities.

The floors of the channels are relatively even and their roughness is moderate, as shown by field studies.

Sediment-free precipitation or meltwater provides the resulting flow (Veress, 2010). The waterflow in the upper part of the channels is likely to be of low turbulence (Trudgill, 1985). The Dachstein limestone in the study area is considered homogeneous (Plan et al., 2009; Veress, 2010). The substrate surface and the interior of the channels are unvegetated.

2.4. DATA FOR CHANNEL DEVELOPMENT

The material transport between the limestone surface and the water significantly increases due to the turbulent waterflow (by eddy diffusion, Dreybrodt, 1988). Due to the turbulent waterflow, the turbulence structure is depicted on the limestone surface. The resulting eddies create various surface shapes (Curl, 1966; Dreybrodt, 1988; Slabe, 1995; Dreybrodt et al., 2005; Covington, 2014; Perne et al., 2014). At the junctions, rivulets entering the rivulet of the main channel cause vorticity, which locally results in a more intense dissolution effect and thus a local hollowing in the main channel at this location (Veress et al., 2013). Since flow velocity also increases at junctions (Veress et al., 2015b), the turbulent transport of mixed material that enters the water by eddy diffusion is also more efficient (Dreybrodt, 1988; Dreybrodt et al., 2005).

3. METHODS

3.1. ANALYSIS OF THE FIELD MORPHOMETRY DATA

The channel cross-section (T^*, Figure 3c, Equation 2) values of individual survey profiles were represented as a function of distance from the lowest point of the main channel (d, Figure 3). This is the $T^*(d)$ function.

The average cross-sectional area (T) and average width-depth ratio (A) values of the local hollowings were calculated. The former is computed by averaging the cross-section areas (T^*) of the individual profiles within the hollowing section (D_T, Figure 3b) as

$$T = \frac{1}{n}\sum_{i=1}^{n} T_i^* \qquad (3)$$

The latter, the average of the calculated width-depth ratios (A^*) is reckoned as

$$A = \frac{1}{n}\sum_{i=1}^{n} A_i^* \qquad (4)$$

In both cases, n means the number of measurement profiles taken at a given local hollowing section (D_T, Figure 3b).

Then, the resulting average width-depth ratio values (A) as a function of the average cross-sectional area (T) are examined. Plotting the data for local hollowings of different size in this way, it is recognized how the average width-depth ratio of the local hollowing changes as its average cross-section increases (i.e., as the channel and local hollowing develop).

The lengths (D_T) of local hollowings measured in the field are examined for junctions with single and multiple tributary channels. Hollowing sections are also grouped according to the average distance of tributary channels from each other (ρ, Figure 3a, 3b). The deviation of D_T section length values from the length of sections of the emerged intense vorticity in the flow (D_S) are examined as a function of ρ.

3.2. SIMULATION

The emerged intense vorticity in the flow was modeled and studied with Computational Fluid Dynamics (CFD, Bates et al., 2005; Jiyuan et al., 2013; Blazek, 2015) simu-
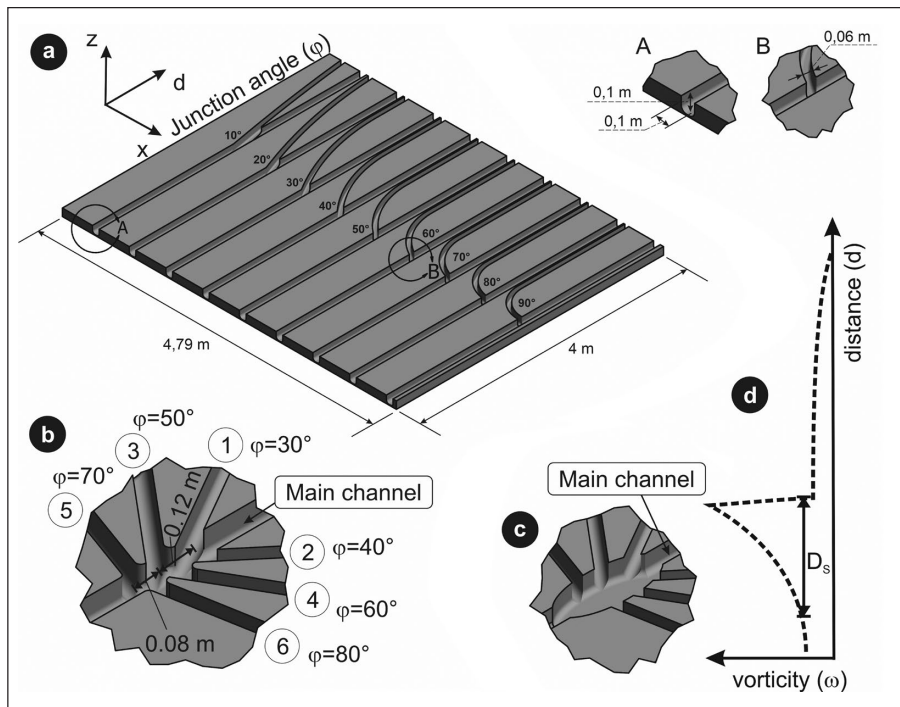
Figure 4: Sketches of digital models used to interpret the observed phenomena in the field. (a) Channel set with single tributary channel junctions; (b) Model with multiple tributary channels, ordinal numbers of tributary channels are marked; (c) Multiple tributary channel model with hollowing part; (d) Value of vorticity as a function of distance.

lation within CAD models (Figure 4). The Navier-Stokes equations (White, 2016) were solved using Xflow code (Holman et al., 2012). This reliable environment was developed for industrial purposes (e.g., Copuroglu & Pesman, 2018) to solve engineering problems.

The code solved the Navier-Stokes equations with the use of the Lattice Boltzmann method (Blazek, 2015). Large Eddy Simulation (LES, Jiyuan et al., 2013) was applied through Wall-Adaptive Local Eddy (WALE, Ducros et al., 1988; Holman et al., 2012) viscosity model for steady-state incompressible flow for constant density and viscosity to model its behavior.

A generalized law of the wall (Shih et al., 1999) that takes into account the effect of adverse and favorable pressure gradients to model boundary layer was applied in the boundary conditions close to the wall. The free surface flow was approximated by particle-based surface tracking method.

The slope angle was set by the change in the components of the gravitational potential. The simulation was set as the steady-state velocity of water entering the computational domain – based on the studies of Szunyogh (1995) and Veress et al. (2015a, 2015b) – was $v=1$ ms^{-1}. Based on the field data, the simulation was carried out between 5°-45° substrate slope angles (α), with α changed in 5° increments per experiment. Data being studied as a result of CFD simulation was the vorticity (ω [s^{-1}]). It is the amount of rotation of a liquid body, which moves with the – also resulting – v velocity vector, and can be defined using the equation

$$\omega = \left| rot\ \underline{v} \right| = \left| \nabla \times \underline{v} \right| \qquad (5)$$

(White, 2016). The representation of ω values with isosurfaces allowed to study the places of intense vorticity and their comparison with model channels. The vorticity (ω) received in the simulation is averaged for a given cross-section in the main channel ($\underline{\omega}$) and is examined as a function of distance (d). By this function, the section the expected length of intense vorticity (D_s, Figure 4d) at the main channel junctions is determined.

Before running the model experiments, a mesh independence test (Bates et al., 2005) was performed, and the optimal simulated time length was determined. Based on these results, a mesh with a resolution of 0.005 m is used for the experiment, and the last 2 seconds of a simulated time interval of 5 seconds are evaluated. To validate the flow velocity (Bates et al., 2005), the laboratory measurements of Veress et al. (2015b) were used, and the simulation was adjusted to match the laboratory measurements of flow velocities.

3.3. APPLIED MODEL CHANNELS
The simulation was applied in a series of three model experiments. Each 3-dimensional model channel was designed in the CAD. These models are simplified representations of field channels.

In the first series of model experiments, the effect of single tributary channel junctions was aimed to investigate. For this purpose, the simulation was applied on a channel set where every individual main channel (9

pieces) was joined with one tributary channel, separately. Different tributary channels join to the main channel individually with junction angles (φ) increasing from left to right with a step of 10° (between 10° to 90°, Figure 4a).

The second set of model experiments is suitable for investigating the effect of tributary channels joining in the vicinity of each other. Here, a distinction is made between asymmetric and symmetric junctions: asymmetric if there is no other junction on the side opposite to the given junction, symmetric if there is. In the five models, the number of tributaries joining the main channel was gradually increased from 2 to 6 per model (Figure 4b, ac-

cording to the numbering of the tributary channels). The distance of the tributary channels is also shown in Figure 4b. Note that the largest distance between the tributary pairs is in the model with 3 and 4 tributaries. In the models with 5 and 6 tributaries, the tributary channels are joined at less than this distance.

For the third set of model experiments, a variation of the previous model channels with a hollowing shape was also designed (Figure 4c). By inserting a hollowing, the vorticity changes in the vicinity of the junctions in the presence of such a feature were investigated.

4. RESULTS

4.1. CROSS-SECTION AND WIDTH-DEPTH RATIO OF LOCAL HOLLOWINGS

First, a simulation with one tributary channel was run. In the simulation, not only the velocity increases at the

junctions, but also the vorticity appears to intensify remarkably for setting any angle of slope and junction (Figure 5a, 5b, 5c). In the junction section, the intense vorticity appears along the edges of the ridges between
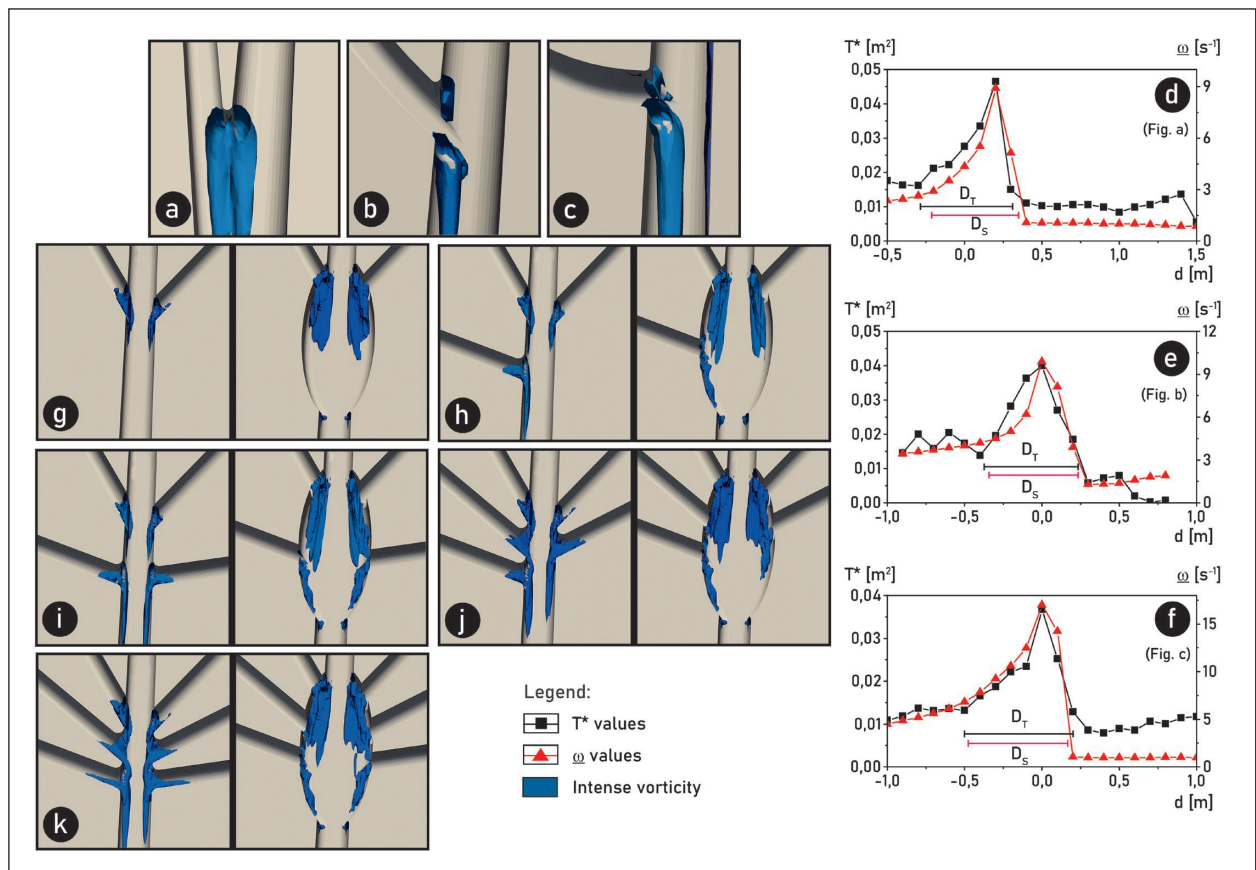

Figure 5: Results of the vorticity of CFD simulation in model channels. (a, b, c) Induced vorticity of tributary channels arriving with junction angles of 10°, 50°, 90° in the model; (d, e, f) The comparison of $\omega(d)$ and $T^*(d)$ functions of sample field channels; (g, h, i, j, k) Model simulations of junctions of two, three, four, five, six tributary channels with hollowing and non-hollowing models.

the channels. After the junction, the value of vorticity gradually decreases.

In the field, local hollowings also appear only along a section. Their cross-sectional area gradually decreases after the junction. Three (sample) simulations are shown as an example in the Figure 5a, 5b, 5c. The cross-section (T^*) values of three selected sample field channels are plotted together with the simulated vorticity (ω) values adjusted with the same slope and junction angle parameters as a function of distance (d) on graphs in Figure 5d, 5e, 5f. The shape of the graphs are similar, the correlations between the data points of the two functions are $R^2 > 0.8$.

When the number of tributaries on a short section of the main channel is increased (Figure 5g, 5h, 5i, 5j, 5k, at the left), more tributaries induce a more extensive vorticity. In all cases, the eddies penetrate the tributary channels over a length of about 0.3 m, so that the eddies

of the simulated waterflow almost surround the ridges between channels. The more tributary channels there are, the more minutely the environment of junctions is divided into ridges between channels. If the junction is symmetric at a given point, the width of the vorticity at that point is larger than that in the asymmetric case.

When the local hollowing develops (this was already investigated in models with hollowing, Figure 3c, Figure 5g, 5h, 5i, 5j, 5k, at right), the only change is that the penetration of vorticity from the main channel into the tributary channel is decreased. Vorticity remains intense at the wall of the local hollowing (including the section between tributary channels). However, in the flow exiting from the dense tributary section, the amount of vorticity in the main channel gradually decreases.

In the field channels (both for single and multiple tributary junctions), a decrease in the average width-depth ratio of the local hollowing (A) is observed with

(A) Average width-depth ratio of a local hollowing
(N) Case number of local hollowings
(T) Average cross-section area of a local hollowing

(B) Number of tributary channels adjoining to a local hollowing
(n) Total case number of tributary channels regarding local hollowings with number B adjoining tributary channels
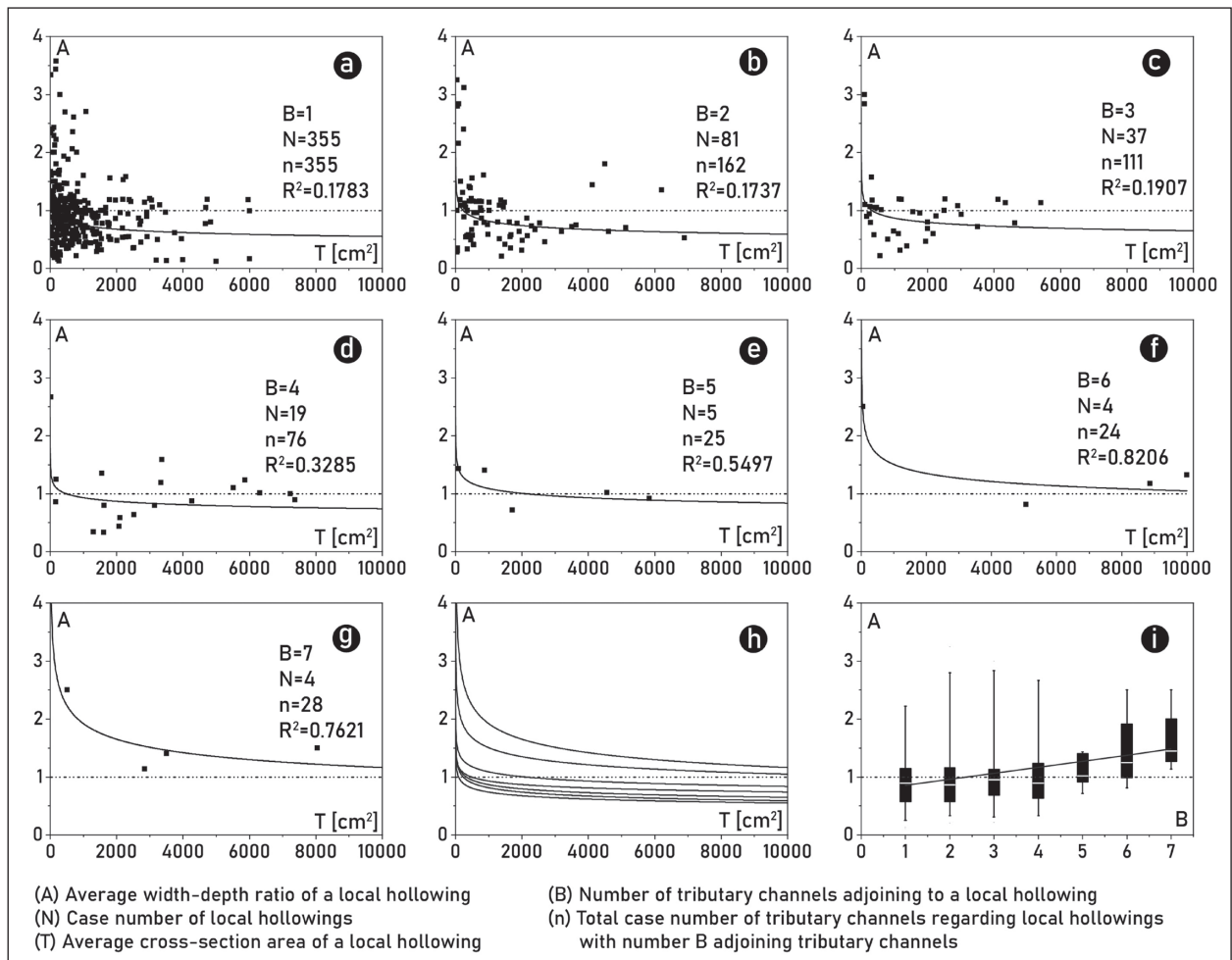
Figure 6: The study of the width-depth ratio of field hollowing parts in main channels due to the effect of the tributary channel junctions. (a-g) The data points of the function A(T) and the power function representing their trend, separated by the number of tributaries joining the local hollowing (B); (h) Summary of power functions describing trends in a common coordinate system; (i) Average width-depth ratio (A) values separated according to the number of tributary channel junctions (B).

increasing average cross-sectional area (T), which initially decreases significantly and then decrease gradually becomes more moderate (Figure 6). The shape of the

$$A(T) = a \cdot T^b \qquad (6)$$

function shows the trend of data points separated by the number of junctions, where a and b are the coefficients in the function. The coefficients of the function are summarized in Table 1. The measured data and the fitted functions representing the trend are presented in Figure 6a, 6b, 6c, 6d, 6e, 6f, 6g.

For field main channels, the functions show that the larger the number of joining tributary channels (B) into common local hollowing, the more moderate the decrease in the average width-depth ratio (A) of the local hollowing (and hence the deepening of the shape). Therefore, as the cross-section increases, the longer time needed for the depth of the local hollowing in the main channel to exceed the width (Figure 6h). When the values for each width-depth ratio (A) are grouped according to the number of tributary channel junctions into a given local hollowing (B) and statistically evaluated (Figure 6i), the more the number of junctions, the wider local hollowing can be found.

Table 1: Coefficients of the power functions plotted in Figure 6.

Number of junctions	a	b	R2
1	1.7873	-0.128	0.1783
2	2. 1405	-0.14	0.1737
3	2.0702	-0.126	0.1907
4	1.8432	-0.099	0.3285
5	2.3914	-0.114	0.5497
6	4.4504	-0.157	0.8206
7	8.6558	-0.218	0.7621

4.2. LENGTH OF LOCAL HOLLOWINGS

The lengths of the intense vorticity sections (D_S) for the single tributary channel junctions are presented in Table 2 based on the $\underline{\omega}(d)$ functions (Figure 4d, Mitre, 2022) for the cases of various slope (α) and junction angles (φ). Previous studies with equivalent simulation (Mitre, 2022) have already found the average values of the D_S and D_T stretches similar. It can also be observed in the graphs of the three field samples in Figure 5d, 5e, 5f, because the stretches of the local maxima of both functions along the d-axis are similar in all three cases.

The graph in Figure 7a (vorticity as a function of distance, $\underline{\omega}(d)$) shows what happens with the intense vorticity section length as the number of tributary channel junctions increases. In Figure 7a, the locations of the local maxima and some of the identifiable intense vorticity section lengths are marked on the graphs.

The results of the experiment with 2 tributary channels (Figure 5g) show that (symmetric) tributaries joining at the same point do not significantly increase the length of the intense vorticity section in comparison with the case of a single tributary channel (Figure 7a). The intensity of the vorticity increases, which gradually decreases with distance from the junction.

The results of the experiments with 3 and 4 tributary channels (Figure 5h, 5i) show that the effect of the tributary channels in the upper position (labelled 1 and 2) results the same trend in the main channel flow as seen in the previous experiment. Then, a new vorticity section is established at the junction of the next tributary channel and a pair of tributary channels (labeled with 5 and 6, Figure 4b, 4c). After that, the intensity of the vorticity again gradually decreases as a function of distance. In the function $\underline{\omega}(d)$ (Figure 7a), two vorticity sections can be separated.

The results of the experiments with 5 and 6 tributary channels (Figure 5j, 5k) show that the intense vorticity

Table 2: Intense vorticity section lengths of local hollowings with single tributary channel for different slope (α) and junction angle (φ) parameters based on the calculation from simulation.

Slope angle (α)	Length of the D_S sections [m]								
	φ=10°	φ=20°	φ=30°	φ=40°	φ=50°	φ=60°	φ=70°	φ=80°	φ=90°
5	0.58	0.38	0.33	0.44	0.58	0.57	1.15	0.95	0.90
10	0.56	0.37	0.31	0.41	0.57	0.53	0.96	0.82	0.76
15	0.55	0.36	0.30	0.39	0.57	0.48	0.77	0.75	0.73
20	0.55	0.35	0.30	0.39	0.57	0.45	0.74	0.72	0.71
25	0.55	0.35	0.29	0.39	0.56	0.44	0.69	0.68	0.66
30	0.55	0.35	0.29	0.39	0.56	0.43	0.66	0.65	0.64
35	0.55	0.35	0.29	0.39	0.55	0.42	0.64	0.64	0.62
40	0.55	0.34	0.28	0.39	0.55	0.41	0.63	0.63	0.62
45	0.54	0.34	0.28	0.38	0.54	0.41	0.61	0.61	0.61

developed at the junctions of intermediate (and short distance) tributary channels (labelled 3 and 4, Figure 4b, 4c) coincides with the vorticity section generated by the lowest tributaries (labelled 5 and 6, Figure 4b, 4c).

Therefore, according to the model experiment with multi-tributary channels, the denser the tributary channels are, the more uniform the vorticity section. The less dense they are, the more they are separated into individual vorticity sections. The similar shape of the $\underline{\omega}(d)$ functions also suggests the length of the vorticity section may be the same as for one tributary channel for cases of sufficiently large distance of tributary channels. Also, symmetrically joining pairs of tributaries at the same point do not change the length of the intense vorticity section, only influence the intensity of the vorticity.

Two types of tributary channel patterns were se-lected in the field in the selected channel system (marked as 1/V/1 in Figure 7b): in one case there are 2 tributaries in the upper position (Area I), and in the other case there are 4 tributaries in the lower position (Area II). In the upper position (Area I), where the distance between tributary channels is larger than the intense vorticity section (D_S) simulated with a single tributary channel, the local hollowings are separated (Figure 7c). In the lower position (Area II), where their distances are less than the length of the intense vorticity section simulated by a sin-gle tributary (D_S), there is a single, non-separated local hollowing (pit-like, Figure 7c).

It can be noticed (Figure 7c) that in the case of Area I, the lengths of the local hollowings (D_T, stretch with dotted line) are similar to the lengths of the simulated vorticity sections (D_S, stretch with continuous line) of
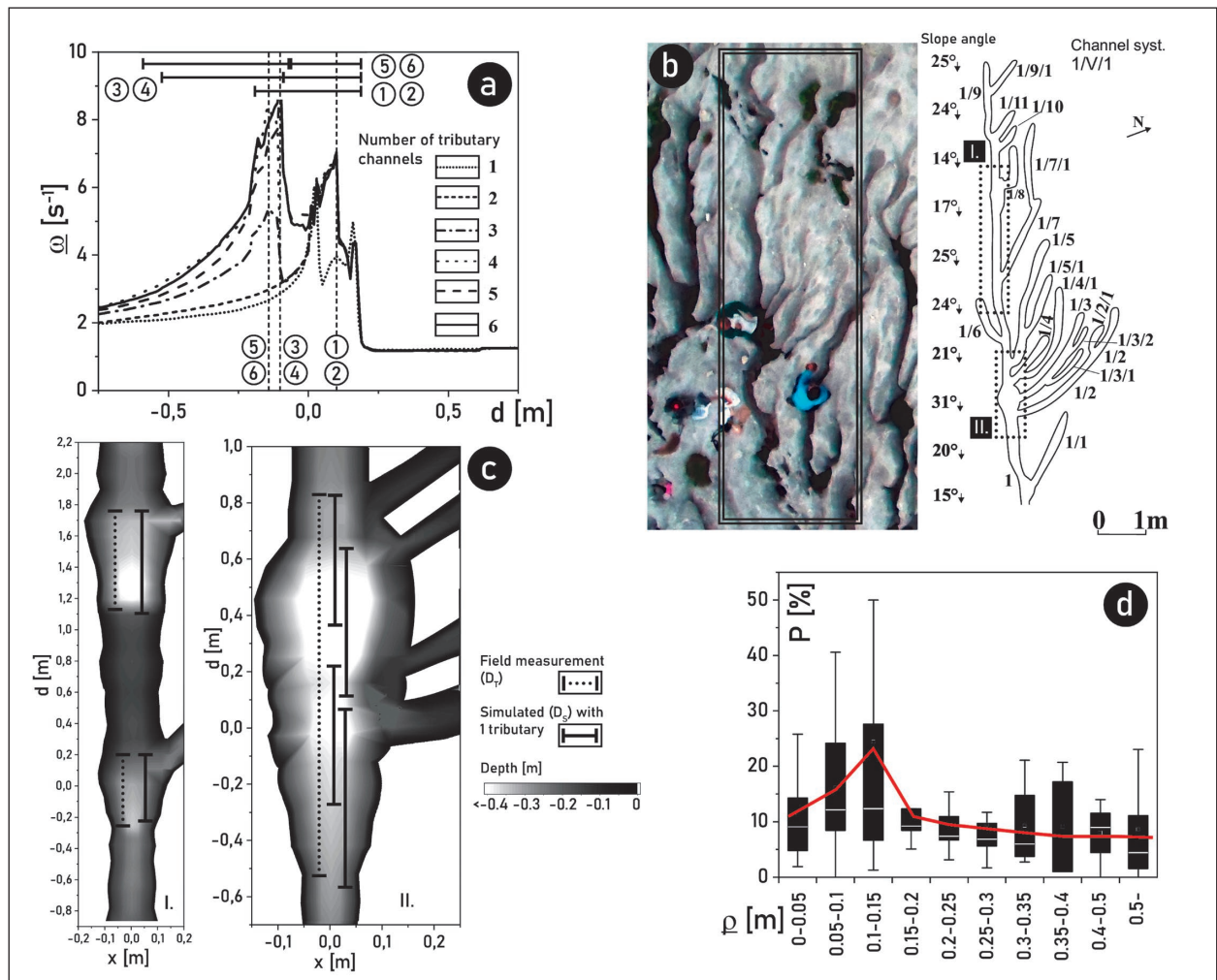

Figure 7: Study of multiple tributary channel junctions. (a) Summary of the $\underline{\omega}(d)$ functions resulting from simulations in the 1-6 tributary CAD model. The numbers indicate the marks of tributary junctions, as shown in Figure 3. The dashed perpendicular lines indicate sites of local maxima; (b) Field channel system and two investigated channel parts within; (c) Maps of the two investigated parts of the field channel system, also including the relative depths; (d) Calculated P values as a function of average tributary channel distance (ϱ) for all junctions under study.

the single tributary channels with the same parameters. While in the case of Area II, only the total length of the local hollowing section can be clearly determined. Here, the separation of the local hollowings caused by each individual tributary channel is uncertain. In other words, in the case of Area II, the measurement of separate D_T sections for each tributary junction in the main channel can be subject to larger errors.

An attempt was made to determine the D_T section length emerging in the main channel at each tributary junction, either directly during the field measurement or during the processing of the field data. Even if it is within a larger local hollowing feature receiving multiple tributaries, such as Area II in Figure 7c.

A value of deviation (P) is introduced to investigate the measured section length (D_T) data:

$$P = \frac{|D_T - D_S|}{D_S} \cdot 100 \qquad (7)$$

which represents the percentage difference between the measured section length (D_T) and the correspondent simulated intense vorticity section length (D_S, Table 2) of single tributary channel junctions. The value of the deviation (P) as a function of the average tributary distance (ϱ) is investigated (Figure 7d). The ϱ average tributary distance means the average distance between the joining tributary channels into a common hollowing feature. When only a single tributary channel is joined to the hollowing feature, the average distance of two closest neighborhood tributary channels (upchannel and downchannel) was reckoned for ϱ (Figure 3a).

On average, the D_T values of the field surveys deviate least from the simulated single tributary channel D_S values in areas with dense and sparse tributary channels, as it can be recognized from in Figure 7d. The deviation is the largest where the average spacing of the tributary channels is moderate (0.1-0.15 m).

5. DISCUSSION

Rinnenkarren evolve under rivulets (Bögli, 1960; Trudgill, 1985; Ford & Williams, 1989). When rivulets join together, local hollowing develops in the main channels around the junctions. The general direction of channel and local hollowing evolution is gradual deepening (Veress et al., 2013). In local hollowing, in addition to growth rate in deepening, the rate of lateral growth is more in-
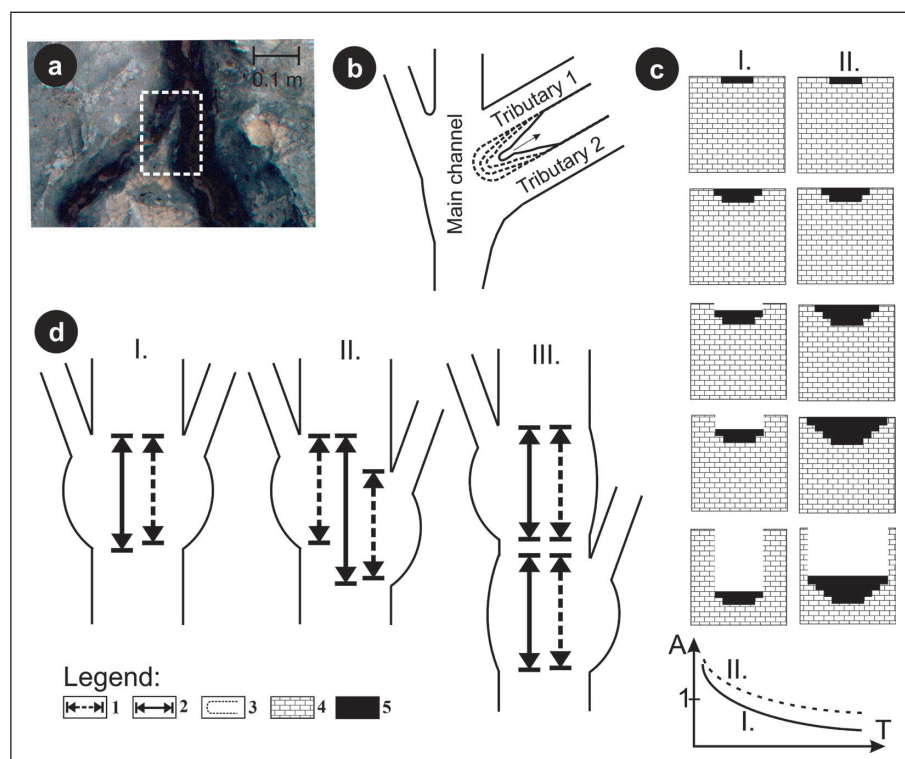

Figure 8: The development of local hollowings. (a) Photo of a ridge between channels; (b) Process of retreating of the ridge between channels at a young junction; (c) Development of the width-depth ratio of a local hollowing at small (I.) and large (II.) water supply, also the shape of the A(T) function; (d) As tributary channels are joined at more distant points, local hollowings become more separated. Legend: (1) Length of intense vorticity section; (2) Measurable length of local hollowing in the field; (3) Previous positions of the ridge between channels; (4) Limestone; (5) Water in the channel.

tense when more tributaries merged within a short main channel section.

Initially, the multiple tributary channels also ensure the widening of the local hollowing with the division of the environment of the main channel into several narrower ridges (Figure 8a). When the local hollowing is not yet, or only partially developed, eddies may also penetrate into the tributary channels along ridges (Figure 5). The ridges shift through dissolution (Figure 8b). The lower end is destroyed during dissolution (Veress, 2010), and the upper part narrows and extends into the undivided surface. This results in the lateral development of the local hollowing. This can be considered widening of the local hollowing by tributary channels. Therefore, the rate of widening also increased in the case of more tributary channels, resulting in a slower decrease in the width-depth ratio (A) of the local hollowing.

According to the model experiment, once the local hollowing is created, vorticity is only present in the main channel. Here, the retreat of the lateral wall of the local hollowing causes the widening. Furthermore, the increase in water volume amplifies this process. Possibility of the latter increases with the emergence of new tributary channels. This results in a more moderate decrease in width-depth ratio (A).

In the field, the function of (6) type (Figure 5) describes the development of the average width-depth ratio (A) of local hollowings, pits, and kamenitzas in the vicinity of the tributary junctions as a function of the average cross-sectional area increase (T). Considering the existing functions, two function shapes are presented as examples (Figure 8c). The more rapidly decreasing function shape (labeled as I, Figure 8c) is associated with constant water supply. While the less rapidly decreasing one (labeled as II, Figure 8c) is associated with increasing water supply. In the latter case, the increasing water supply results in a more intensive widening and hence a larger width-depth ratio (Figure 8c, graph).

On average, local hollowings that receive 5 or less tributary channels (since $A<1$, Figure 6) develop into a pit in the developed state based on the function analysis of field data (Figure 6). Local hollowings receiving 6-7

tributaries develop into kamenitzas (as $A>1$, Figure 6). After further (even long) development, these kameniztas may even reach the width-depth ratio $A<1$ (Figure 6).

The vorticity of the rivulet exiting the local hollowing is gradually fragmented downstream in the main channel (Figure 5, 7a). Its influence on the development of the cross-section is reduced accordingly. Leaving the local hollowing, the cross-section of the main channel is smaller than that at the local hollowing. Therefore, the section length of the local hollowing can be detected and measured in the field (Figure 5d, 5e, 5f, 7c).

The junction distance of the tributary channels determines the pattern of local hollowings and their section length in the main channel (Figure 8d). If the tributary channels are joined very close (<0.1 m) to each other, a single local hollowing is resulted. Its measurable length in the field does not differ significantly from the vorticity section length determined by the model experiment for a single tributary channel junction (Figure 8d, case I.).

When the distance between the tributary junctions is increased (Figure 8d, case II.), the induced local hollowings of each tributary in the main channel are already slightly separated. The greater the distance between the tributary channels, the greater this separation. In field surveys, in such cases, stretches of local hollowings from individual tributary channels are difficult to identify (Figure 7c). In the field, it is possible to measure only the total length of the local hollowing section containing all the tributaries. Therefore, in similar cases, the length of each local hollowing measured in the field may differ significantly from the vorticity section length measured in the model experiment for a single tributary channel junction.

When the tributary channel junction distances exceed the intense vorticity section lengths that each individual tributary channel induces (based on the model simulation, according to the Table 2), the local hollowing section length can develop along its entire length (Figure 8d, case III.). The beginning and end point of the local hollowing can be detected during the field survey, so also a low deviation affects the measurement of the section length.

6. CONCLUSIONS

The cross-section of the rinnenkarren gradually increases in the downstream direction. This continuous increase is sectionally subdivided by local hollowings, pits, and kamenitzas at the tributary channel junctions.

As throughout the channel, the general development trend of the channel cross-section at the junctions is also deepening. Thus, the evolved local hollowing at the initial stage develops into a pit over time. However, the more tributary channels are joined in close vicinity to each other, the greater the lateral growth (widening) rate

of the channel cross-section and a kamenitza-like feature develops.

The appearing vorticity in channel systems can be studied by simulation model experiments. By comparing the latter with the corresponding field data, the evolution of local hollowings can be more accurately described. In the field channel, the local hollowing (or pit and kamenitza) is a continuous downstream feature along stretches with a high density of tributary channels. Taking into account the vorticity sections obtained in the model experiment, the potentially continuous hollowing gradually subdivides into individual local hollowings as the density of tributary channels decreases. Once the separation of field tributaries exceeds a distance of one meter, the individual local hollowing sections are completely separated.

Model experiments show that a smaller scale of vorticity is also present in the other non-hollowing sections of the channels. This is due to the flow characteristics of the rivulet. This also results in a moderate increase in the channel cross-section between local hollowing sections, as described by previous research.

REFERENCES

Bates, P.D., Lane, S.N., Ferguson, R.I., 2005. Computational Fluid Dynamics, Applications in Environmental Hydraulics. John Wiley & Sons Ltd., 540 pp. https://doi.org/10.1002/0470015195

Blazek, J., 2015. Computational Fluid Dynamics: Principles and Applications, Third Edition. Butterworth-Heinemann, Elsevier, 447 pp. https://doi.org/10.1016/C2013-0-19038-1

Bögli, A., 1960. Kalklösung und Karrenbildung. Zeitschrift für Geomorphologie, Suppl. 2: 4-21.

Cooper, M.P., Covington, M.D., 2020. Modeling cave cross-section evolution including sediment transport and paragenesis. Earth Surface Processes and Landforms, 45(11): 2588-2602. https://doi.org/10.1002/esp.4915

Copuroglu, H.I., Pesman, E., 2018. Analysis of Flettner Rotor ships in beam waves. Ocean Engineering, 150: 352–362. https://doi.org/10.1016/j.oceaneng.2018.01.004

Covington, M.D., 2014. Calcite dissolution under turbulent flow conditions: a remaining conundrum. Acta Carsologica, 43(1): 195-202. https://doi.org/10.3986/ac.v43i1.628

Covington, M.D., Perne, M., 2015. Consider a cave: a physicist's view of cave and karst science. Acta Carsologica, 44(3): 363–380.

Curl, R.L., 1966. Scallops and flutes. Transactions of the Cave Research Group of Great Britain, 7(2): 121–160.

Deák, Gy., Samu, Sz., Péntek, K., Mitre, Z., Veress, M., 2012. Vízáramlási modellkísérletek vályúrendszereken. Karsztfejlődés, XVII: 155-163.

Dreybrodt, W., 1988. Processes in Karst Systems. Physics, Chemistry, and Geology. Springer-Verlag Berlin, Heidelberg, 288 pp. https://doi.org/10.1007/978-3-642-83352-6

Dreybrodt, W., Gabrovšek, F., Romanov, D., 2005. Processes of Speleogenesis: A Modeling Approach. ZRC Publishing, Karst Research Institute at ZRC SAZU, 375 pp.

Ducros, F., Franck, N., Poinsot, T., 1998. Wall-adapting local eddy-viscosity models for simulations in complex geometries. In: Baines, M.J. (Ed.), Proceedings of 6th ICFD Conference on Numerical Methods for Fluid Dynamics, pp. 293-299.

Ford, D.C., Williams, P.W., 1989. Karst Geomorphology and Hydrology. Unwin Hyman, London, 601 pp.

Ford, D.C., Williams, P.W., 2007. Karst Hydrogeology and Geomorphology. John Wiley & Sons, Chichester, 561 pp. https://doi.org/10.1002/9781118684986

Holman, D.M., Brionnaud, R.M., Abiza, Z., 2012. Solution to industry benchmark problems with the Lattice-Boltzmann code Xflow. In: Eberhardsteiner, J. et al. (Eds.), European Congress on Computational Methods in Applied Sciences and Engineering (ECCOMAS 2012), 22 pp.

Hutchinson, D.W., 1996. Runnels, rinnenkarren and mäanderkarren form, classification and relationship. In: Fornós, I.J., Ginés, A. (Eds.), Karren Landforms. Universitat de les Illes Balears, Palma de Mallorca, pp. 209-223.

Jiyuan, T., Guan-Heng, Y., Chaoqun, L., 2013. Computational Fluid Dynamics - A Practical Approach. Second edition, Elsevier Ltd. United Kingdom, 440 pp. https://doi.org/10.1016/C2010-0-67980-6

Mitre, Z., 2022. Effects of the tributary channel and water catchment area on rinnenkarren development (Totes Gebirge, Austria). Physical Geography, 25 pp. https://doi.org/10.1080/02723646.2022.2127477

Perne, M., Covington, MD., Myre, J., 2014. Modeling of bedrock channel and cave evolution using computa-

tional fluid dynamics. 2014 GSA Annual Meeting in Vancouver, British Columbia, 20 pp.

Plan, L., Filipponi, M., Behm, M., Seebacher, M., Jeatter, P., 2009. Constraints on alpine speleogenesis from cave morphology – a case study from the eastern totes gebirge (Northern Calcareous Alps, Austria). Geomorphology 106(1–2): 118–129. https://doi.org/10.1016/j.geomorph.2008.09.011

Shih, T.H., Povinelli, L.A., Liu, N.S., Potapczuk, M.G., Lumley, J.L., 1999. A Generalized Wall Function. National Aeronautics and Space Administration Glenn Research Center, USA. NASA TM-1999-209398 ICOMP-99-08, 16 pp.

Slabe, T., 1995. Cave Rocky Relief. Znaustvenaraziskoval-ni Center SAZU, Ljubljana, 128 pp.

Sweeting, M.M., 1973. Karst Landforms. Columbia University Press, New York, 362 pp.

Szunyogh, G., 1995. Karrvályúk vízszállító-képességének elméleti meghatározása. Karsztfejlődés, I: 133-144.

Trudgill, S.T., 1985. Limestone geomorphology. Longman, New York, 196 pp.

Veress, M., 2010. Karst Environments – Karren Formation in High Mountains. Springer, Dordrecht Heidelberg, London New York, 230 pp. https://doi.org/10.1007/978-90-481-3550-9

Veress, M., 2016. Covered Karst. Springer, Berlin, Heidelberg, New York, 536 pp. https://doi.org/10.1007/978-94-017-7518-2

Veress, M., Zentai, Z., Péntek, K., Mitre, Z., Deák, Gy., Samu, Sz., 2013. Flow dynamics and shape of rinnenkarren systems. Geomorphology, 198: 115-127. https://doi.org/10.1016/j.geomorph.2013.05.019

Veress, M., Samu, Sz., Mitre, Z., 2015a. The effect of slope angle on the development of type a and type b channels of rinnenkarren with field and laboratory measurements. Geomorphology, 228: 60-70. https://doi.org/10.1016/j.geomorph.2014.08.014

Veress, M., Samu, Sz., Széles, Gy., Döbröntei, L., Zentai, Z., Mitre, Z., 2015b. The development of rinnenkarren systems. Karsztfejlődés, XX: 101-124.

Veress, M., Telbisz, T., Tóth, G., Lóczy, D., Ruban, D.A., Gutak, J.M., 2019. Glaciokarsts. Springer, Cham, Switzerland, 516 pp. https://doi.org/10.1007/978-3-319-97292-3

White, W.B., 1988. Geomorphology and Hydrology of Karst Terrains. Oxford University Press, New York, Oxford, 464 pp.

White. F.M., 2016. Fluid mechanics. McGraw-Hill Education - Eighth Edition, 848 pp.

Zhao, Y., Liao, W., Lei, X., 2019. Hydrological Simulation for Karst Mountain Areas: A Case Study of Central Guizhou Province. Water, 11(5): 991. https://doi.org/10.3390/w11050991